Oscillations of the collisionless sheath at grazing incidence of the magnetic field

M. Shoucri, H. Gerhauser, and K. H. Finken

Citation: Physics of Plasmas **16**, 103506 (2009); doi: 10.1063/1.3250290
View online: http://dx.doi.org/10.1063/1.3250290
View Table of Contents: http://scitation.aip.org/content/aip/journal/pop/16/10?ver=pdfcov
Published by the AIP Publishing

Oscillations of the collisionless sheath at grazing incidence of the magnetic field

M. Shoucri,[1] H. Gerhauser,[2] and K. H. Finken[2]
[1]*Institut de Recherche d'Hydro-Québec, Varennes, Québec J3X 1S1, Canada*
[2]*Institut für Plasmaphysik, Forschungszentrum Jülich, D-52425 Jülich, Germany*

(Received 21 July 2009; accepted 21 September 2009; published online 28 October 2009)

An Eulerian Vlasov code is used to study the physics of a collisionless sheath with grazing angles of incidence of the magnetic field. The electrons are treated with a parallel-*B* kinetic equation. In the case where the ion gyroradius is large compared to the Debye length, the electrons, frozen by the magnetic field line, have to move rapidly along the magnetic field *B* in their attempt to follow the ions gyrating perpendicular to *B*. Below a critical angle of incidence of the magnetic field, the large gyroradius ions can be scraped off at the plasma-wall interface of the sheath. The electrons now determine the characteristic time for information propagation, with low frequency oscillations appearing in the system. In the case where the ion gyroradius is reduced to the same order as the Debye length, the results evolve closer to those of the classical sheath, and the amplitude of the low frequency oscillations is reduced. © *2009 American Institute of Physics*. [doi:10.1063/1.3250290]

I. INTRODUCTION

A study of the plasma-wall transition problem in a configuration where the external magnetic field is at grazing incidence to the wall is important in many physical situations. In such a configuration the particles and heat flow to the material surface are critically dependent on the sheath characteristics. Understanding the physical processes that are at play in this situation is important to understand probe characteristics (see, for instance, the work in Ref. 1). In fusion devices, this problem is important to determine the heat load on the limiter or divertor in many plasma-limited or diverted transitions in tokamaks. Also, the scrape-off layer, which is in contact with the wall, can erode the surface and release high-*Z* impurities which migrate toward the confined tokamak plasma (see, for example, Ref. 2). In low pressure plasmas, the problem of understanding the physics of the plasma-wall transition for treating material surfaces is at the heart of an industrial revolution whose theme is the design of matter on the molecular scale.

It is well known in the case of a nonmagnetized plasma that the condition for the sheath formation demands that the ions enter the sheath region at the sheath entrance after being accelerated to the sound velocity in a collisional presheath region. This is known as the Bohm criterion. This problem has been investigated in several publications (see, for instance, Refs. 3–7). When a magnetic field is applied, the ion Larmor radius ρ_i governs the physical phenomena related to the magnetic field, as discussed, for instance, in Refs. 8 and 9. The case where $\rho_i \gg \lambda_{De}$, where λ_{De} is the Debye length, has been considered in several publications (see, for instance, Refs. 9–11). It was shown in this case that a new intermediate region exists between the sheath (also called the Debye sheath) and the collisional presheath in order to redirect the ionic flow guided by the magnetic field toward the wall. This region is the magnetic presheath, whose spatial extension depends on the gyroradius ρ_i and is determined by a competition between the magnetic field, which tends to keep the gyrating ions guided along the field lines, and the sheath electric field, which tends to reorient them along the direction normal to the wall. In Ref. 11, the authors did a careful study to distinguish between these three different regions, i.e., the Debye sheath, the magnetic presheath region, and the collisional presheath. Their conclusion was that for strong magnetic field cases, the thickness of the magnetic presheath is of the same order as the Debye sheath, the parallel and perpendicular velocities are of the same order of magnitude, and thus the plasma-wall transition can no longer be clearly divided into three separate regions, especially at grazing incidence of the magnetic field. Also, the Bohm's criterion at the entrance of the Debye sheath cannot be satisfied when the magnetic field is large and the incidence is at grazing angle (see also the results in Ref. 12).

The simulations presented in Refs. 9 and 11 were done using an adiabatic equation for the electrons. This model resulted in steady-state equilibrium solutions for the sheath problem, at angles of incidence of the magnetic field that are not very small. However, it has recently been shown in Ref. 13 that for strong magnetic fields and small grazing angles of incidence, steady-state oscillations can take place at the plasma-wall transition, and that a kinetic equation has to be used for the electrons to accurately and properly study these oscillations. It is the purpose of the present work to present kinetic simulations of the sheath problem for the case of a strong magnetic field and small grazing angles of incidence when the ion gyroradius is much larger than the Debye length. The kinetic response of the electrons in their motion along the magnetic field lines, responding to the gyrating ions, is important and requires a parallel-*B* kinetic equation for the electrons, which are frozen along the magnetic field lines. For the case of a large ratio of the ion gyroradius to the Debye length, there is a mechanism other than transport that brings the ions into contact with the wall at small grazing angles of incidence of the magnetic field, namely, the ions gyrating around the magnetic field can be scraped off by the

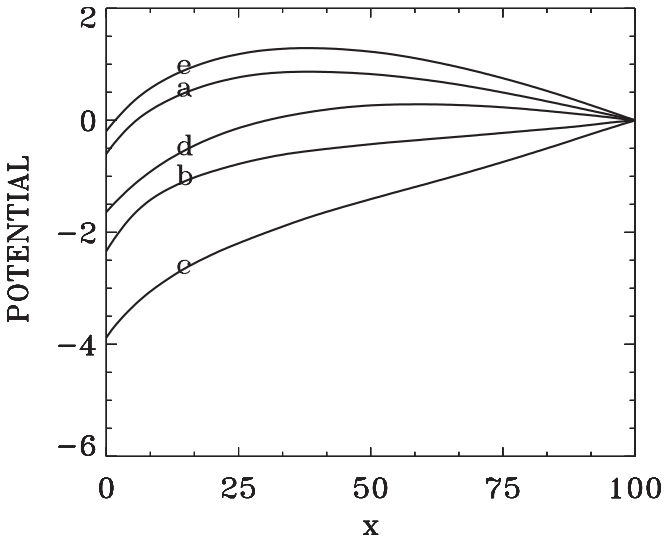

FIG. 1. Potential profile at (a) $t=350$, (b) $t=375$, (c) $t=400$, (d) $t=425$, and (e) $t=450$.

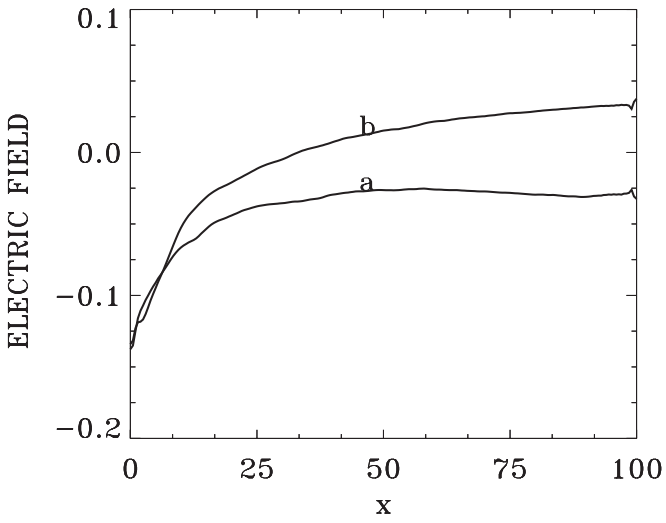

FIG. 2. Electric field at (a) $t=400$ and (b) $t=450$.

wall, as discussed in Ref. 13. The electrons, frozen by the magnetic field, run along the magnetic field in their attempt to catch the ions gyrating across the magnetic field. Below a critical angle of incidence of the magnetic field, the electrons then determine the characteristic times for information propagation. This results in low frequency steady-state oscillations appearing in the sheath, which are not related to edge turbulence. We are far in this case from the picture of an equilibrium solution for the sheath with an adiabatic law for the electrons. The charge separation at a sheath-wall transition is very sensitive to the effect of the finite ion gyroradius or, more precisely, to the ratio of the ion gyroradius to the Debye length. The entire domain will be called the sheath domain since in this case it is not possible to distinguish between different regions, as we previously mentioned, and the ions guided by the magnetic field have an important motion along the magnetic field in addition to the gyration across the magnetic field.

We use an Eulerian Vlasov code in one spatial dimension in which the electrons, assumed to move only along the magnetic field lines, are described by a parallel-B kinetic equation, whereas the ions are described by a kinetic equation in the full velocity space, which integrates exactly the ion orbits in the four-dimensional phase-space considered. A deuterium plasma is considered. The equations are solved numerically using a method of fractional step, which has been previously discussed in literature (see, for instance, Ref. 14).

II. THE KINETIC MODEL FOR THE SHEATH

The relevant equations are those presented in Ref. 13. We present these equations in order to fix the notation. We consider a one-dimensional (1D) slab geometry in which the inhomogeneous direction is in the x-direction normal to the wall. The y-and z-directions are assumed homogeneous. The constant magnetic field is located in the (x,y)-plane and makes a small angle α with the y axis. The magnetized electrons are restricted to move with a velocity $v_\parallel$ along the magnetic field and are described using a kinetic equation in the direction along the magnetic field, with a distribution function $f_e(x,v_\parallel,t)$ obeying the following Vlasov equation:

$$\frac{\partial f_e}{\partial t} + v_\parallel \sin\alpha \frac{\partial f_e}{\partial x} - \frac{m_i}{m_e} E_x \sin\alpha \frac{\partial f_e}{\partial v_\parallel} = 0. \tag{1}$$

Time is normalized to the ion plasma frequency ω_{pi}^{-1}, velocity is normalized to the acoustic velocity $c_s=\sqrt{T_e/m_i}$, and length is normalized to Debye length $\lambda_D=c_s/\omega_{pi}$. The potential is normalized to T_e/e and the density is normalized to the peak initial central density n_0. The ions are treated with a kinetic Vlasov equation in one spatial dimension, which is written for the distribution function $f_i(x,v_x,v_y,v_z,t)$ as

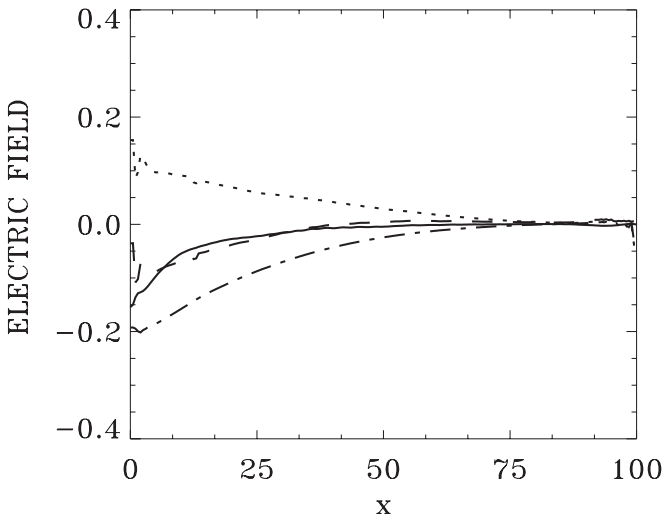

FIG. 3. Electric field at $t=375$ (full curve), $\nabla P_i/n_i$ (dotted curve), $0.1\langle v_z\rangle/\cos\alpha$ (dash-dot curve), and $\nabla P_i/n_i+0.1\langle v_z\rangle/\cos\alpha$ (dash curve).

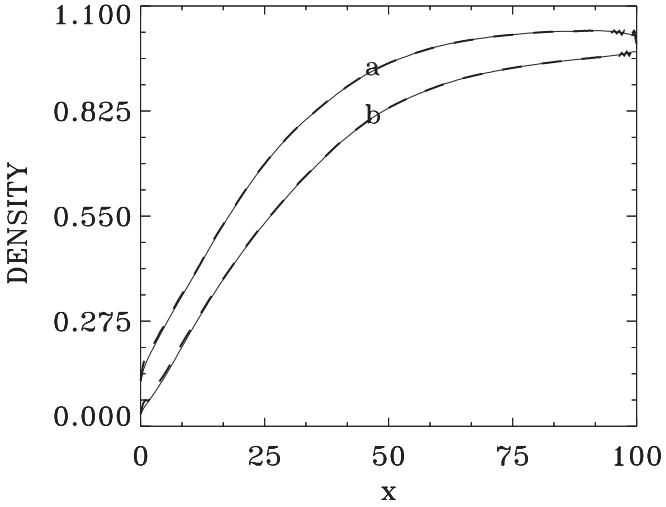

FIG. 4. Density profiles (full curve electrons, broken curve ions) at (a) $t=400$ and (b) $t=450$.

$$\frac{\partial f_i}{\partial t} + v_x \frac{\partial f_i}{\partial x} + (E_x - v_z \omega_{ci} \cos \alpha) \frac{\partial f_i}{\partial v_x} + v_z \omega_{ci} \sin \alpha \frac{\partial f_i}{\partial v_y} + \omega_{ci}(v_x \cos \alpha - v_y \sin \alpha) \frac{\partial f_i}{\partial v_z} = 0, \tag{2}$$

where ω_{ci} is the ions gyrofrequency (normalized to ω_{pi}). The electric field is calculated from the following Poisson equation:

$$\frac{\partial^2 \phi}{\partial x^2} = -(n_i - n_e), \quad E_x = -\frac{\partial \phi}{\partial x}, \tag{3}$$

where

$$n_i(x) = \int f_i(x, \vec{v}) d\vec{v},$$

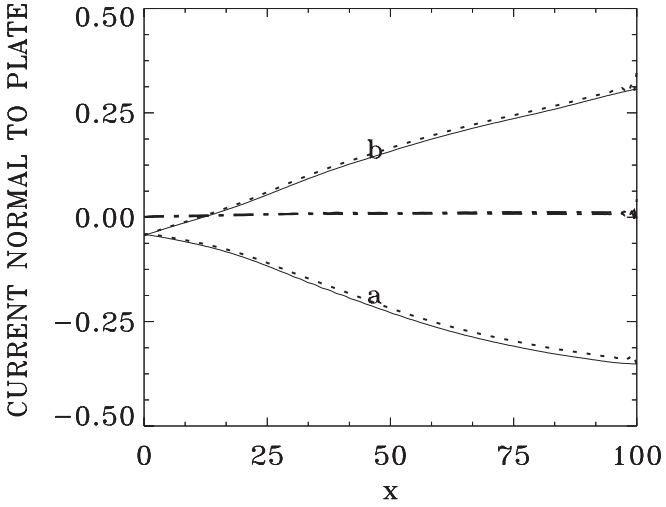

FIG. 5. Current normal to plate (full curve electrons, dotted curve ions) at (a) $t=375$ and (b) $t=425$ (the dash-dot curve is the total current, essentially zero).

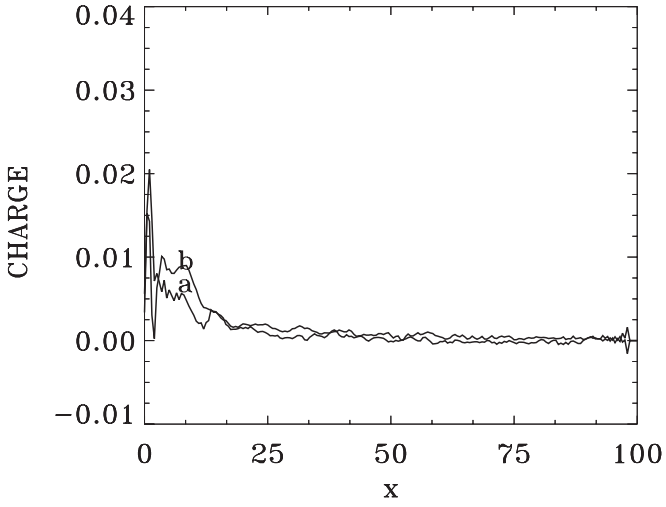

FIG. 6. Charge $(n_i - n_e)$ at (a) $t=400$ and (b) $t=450$.

$$n_e(x) = \int f_e(x, v_\parallel) dv_\parallel.$$

In the present work, we assume a completely absorbing wall at $x=0$. We consider that the right boundary at $x=L$ is a sheath edge or sheath entrance, where ions are in-streaming from a similar plasma that extends beyond $x=L$. We study how the kinetic electrons and ions adjust accordingly in the sheath domain, starting from the following initial conditions. At the sheath entrance $x=L$, the in-streaming ions have initially a parallel to B shifted Maxwellian distribution of the form (see Refs. 9 and 13 for more details)

$$f_i(L, \vec{v}) \sim \frac{g(v_\parallel)}{(2\pi/t_{ei})^{3/2}} e^{-t_{ei}(v_\parallel - v_0)^2/2} e^{-t_{ei}(v_\perp^2 + v_z^2)/2}, \tag{4}$$

with $t_{ei}=T_e/T_i$. $v_\parallel$ is the velocity component parallel to the magnetic field and $v_\perp$ is the velocity component normal to the magnetic field. The shift v_0 is chosen *initially* to be the

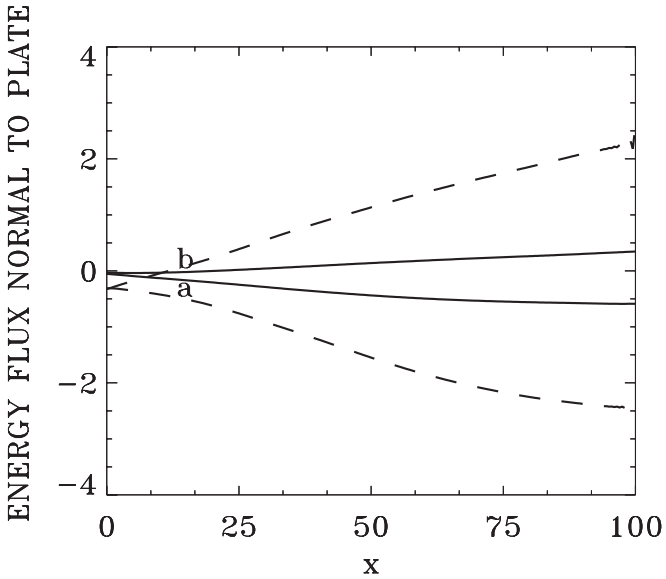

FIG. 7. Energy flux normal to plate (Q_e full curves, Q_i dash curves) at (a) $t=375$ and (b) $t=425$.

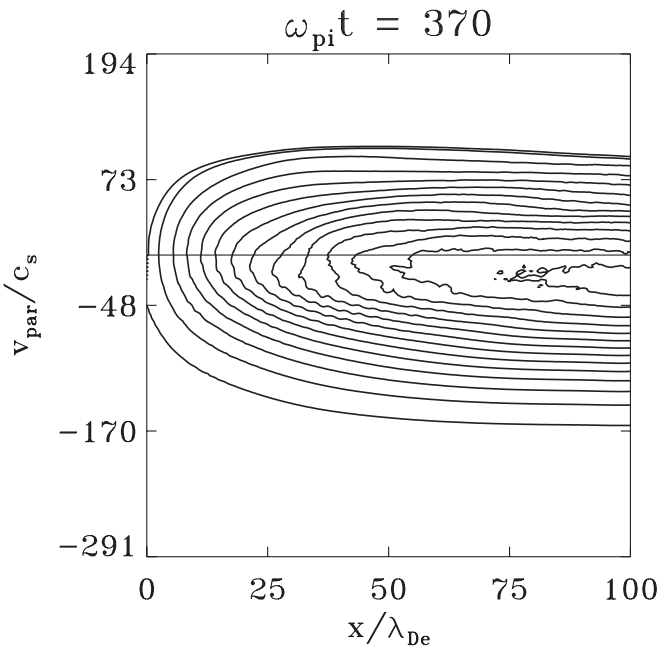

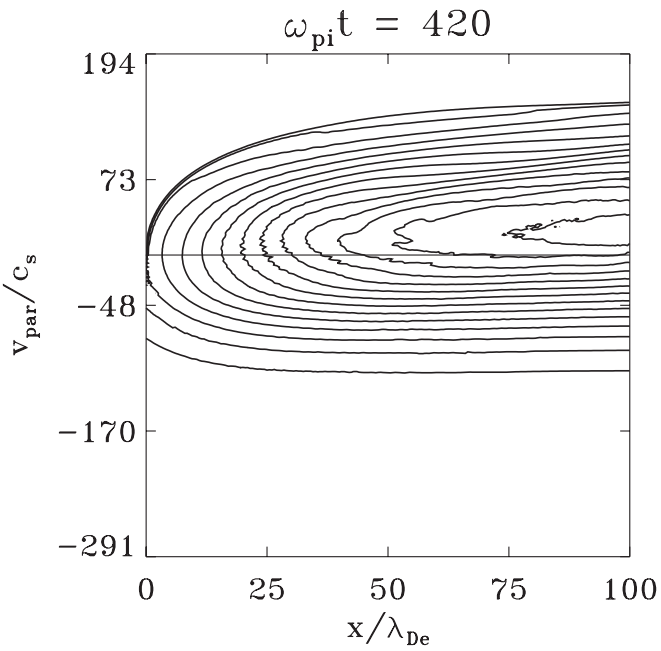

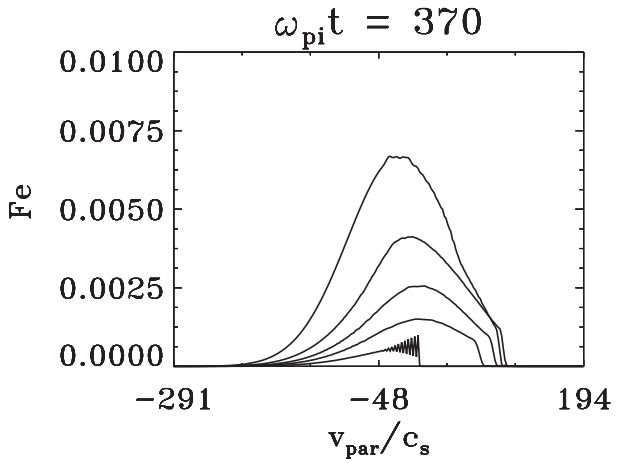

FIG. 8. Electron distribution functions at $t=370$.

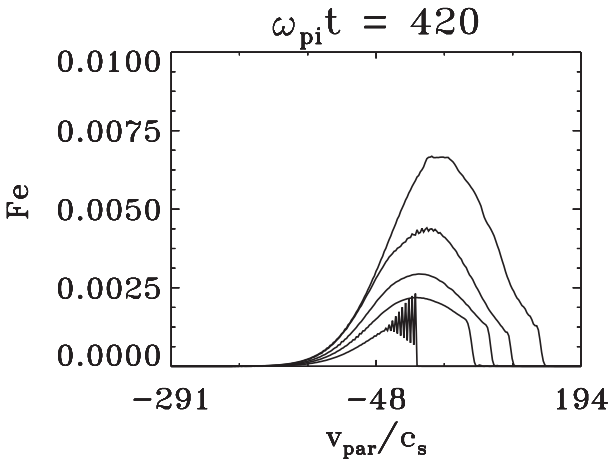

FIG. 9. Electron distribution functions at $t=420$.

negative sound velocity $\sqrt{1+1/t_{ei}}$. The velocity of the instreaming ions is left to evolve during the simulation by assuming that a similar plasma extends beyond $x=L$. The smoothing factor $g(v_\parallel)=[1-\exp(-2t_{ei}v_\parallel^2)]$ is chosen to provide initially a smooth transition to $f_i=0$ for $v_\parallel>0$. The electron distribution function $f_e(x=L,v_\parallel,t=0)$ at $x=L$ is initially taken as a Maxwellian,

$$f_e(x=L,v_\parallel,t=0)=N_e\exp[-m_e v_\parallel^2/(2m_i)] \tag{5}$$

normalized and truncated at a velocity V_c such that its density and its current are equal to the density and current obtained from Eq. (4). V_c is determined as follows. We assume that initially at the right boundary the injected ions have a density $n_i(x=L)=\int_{-\infty}^{0} f_i(\vec{v})d\vec{v}$. The initial density of the electrons at the right boundary should be equal to the density n_i. Using Eq. (5),

$$n_i=\int_{-\infty}^{V_c} f_e(v_\parallel)dv_\parallel$$

$$=N_e\sqrt{\frac{\pi m_i}{2m_e}}\left[\operatorname{erf}\left(V_c\Big/\sqrt{\frac{2m_i}{m_e}}\right)+1\right], \tag{6}$$

where

$$\operatorname{erf}(y)=\frac{2}{\sqrt{\pi}}\int_0^y e^{-y^2}dy$$

is the error function. Equation (6) gives a first relation between N_e and V_c. The ion current density at $x=L$ penetrating the plasma in the direction parallel to B: $j_i=\int_{-\infty}^{0} v_\parallel f_i(\vec{v})d\vec{v}$ (which is negative, the ions are injected at $x=L$ toward the left in the plasma), must be equal to the electron current density along the magnetic field B at $x=L$: $j_e=\int_{-\infty}^{V_c} v_\parallel f_e(v_\parallel)dv_\parallel$. Substituting for f_e from Eq. (5), we arrive after some straightforward algebra at the following transcendental equation for V_c:

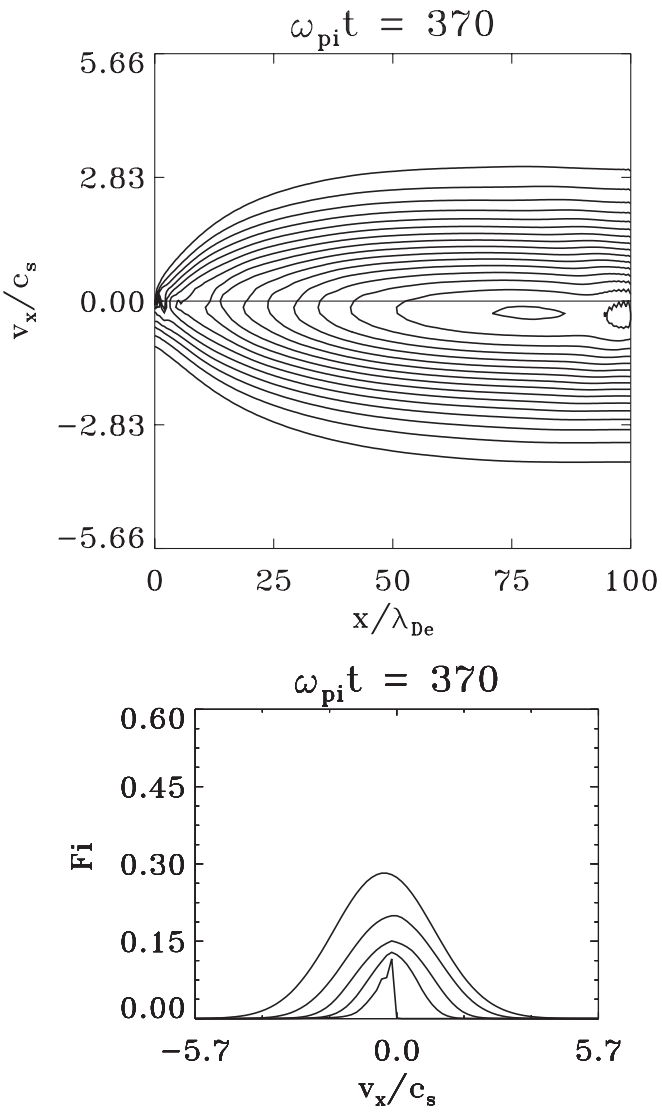

FIG. 10. Ion distribution functions $F_i(x,v_x)$ at $t=370$.

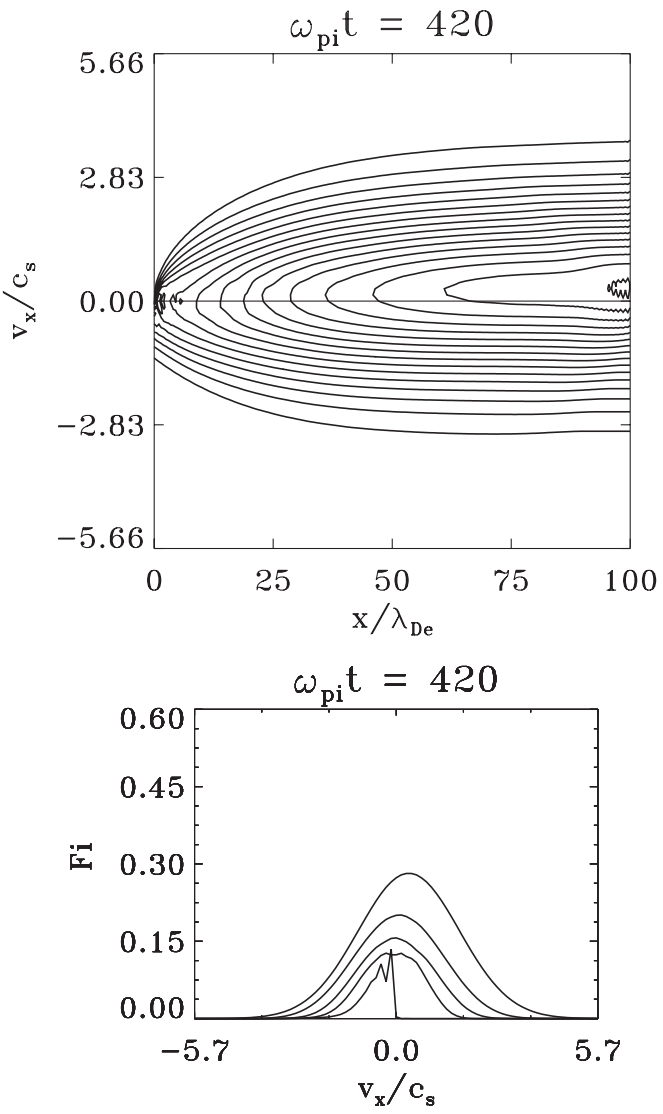

FIG. 11. Ion distribution functions $F_i(x,v_x)$ at $t=420$.

$$\frac{j_i}{n_i} = -\sqrt{\frac{2m_i}{\pi m_e}}\frac{e^{-m_e V_c^2/2m_i}}{\mathrm{erf}\left(V_c\sqrt{\frac{m_e}{2m_i}}\right)+1}, \tag{7}$$

which is solved numerically for V_c. This allows the electron density and current along the magnetic field at the sheath entrance $x=L$ to be equal to the ion density and current along the magnetic field at $x=L$ (see for more details Refs. 9 and 13). The initial condition in the domain is taken to be spatially uniform with $f_{i,e}(x,\vec{v})=f_{i,e}(L,\vec{v})$. $m_{ei}=m_e/m_i=0.5/1836$ for deuterium. We assume a completely absorbing wall at $x=0$, and that at the sheath entrance at the right boundary at $x=L$, the plasma extends to an identical plasma so that the point next to the last grid point is identical to the last grid point. At the left boundary at $x=0$, particles hitting the wall are lost from the system and collected through the current delivered at the plate,

$$\left.\frac{\partial E_x}{\partial t}\right|_{x=0} = -J_x|_{x=0} = -(J_{xi}-J_{xe})|_{x=0}, \tag{8}$$

from which

$$E_x|_{x=0} = -\int_0^t J_x|_{x=0}dt \equiv -\left.\frac{\partial\phi}{\partial x}\right|_{x=0}, \tag{9}$$

where

$$\vec{J}_i = \int d\vec{v}\vec{v}f_i(x,\vec{v}),$$

$$J_{e\|} = \int dv_\| v_\| f_e(x,v_\|)$$

and $J_{xe}=J_{e\|}\sin\alpha$. We integrate over the domain the equation $\partial E_x/\partial x=(n_i-n_e)$ and we get

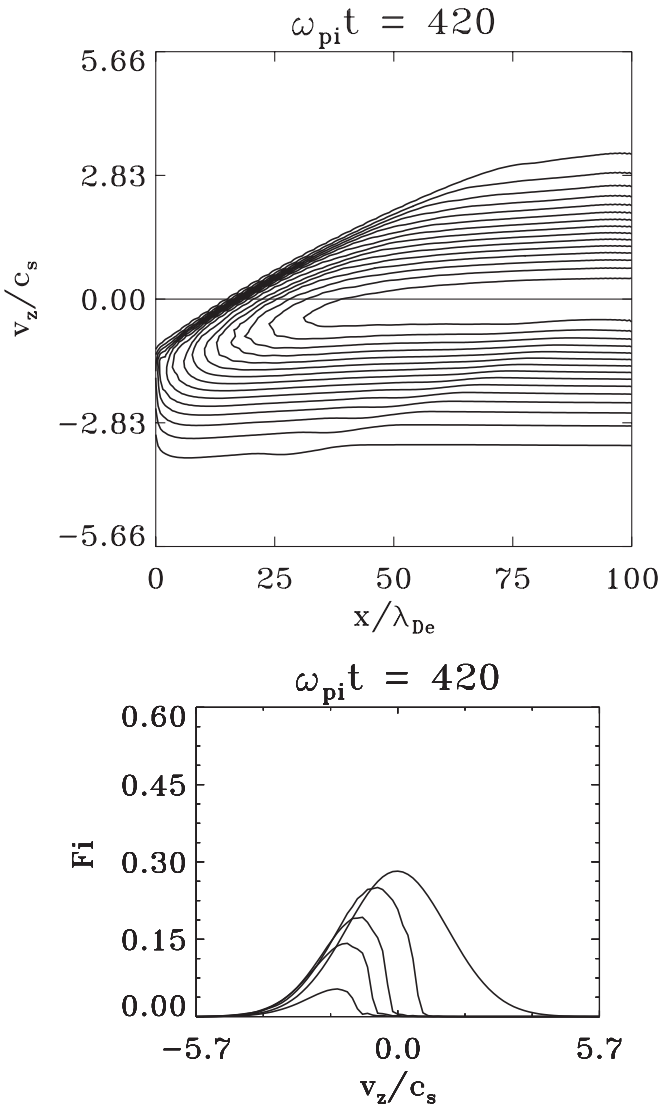

FIG. 12. Ion distribution functions $F_i(x,v_z)$ at $t=420$.

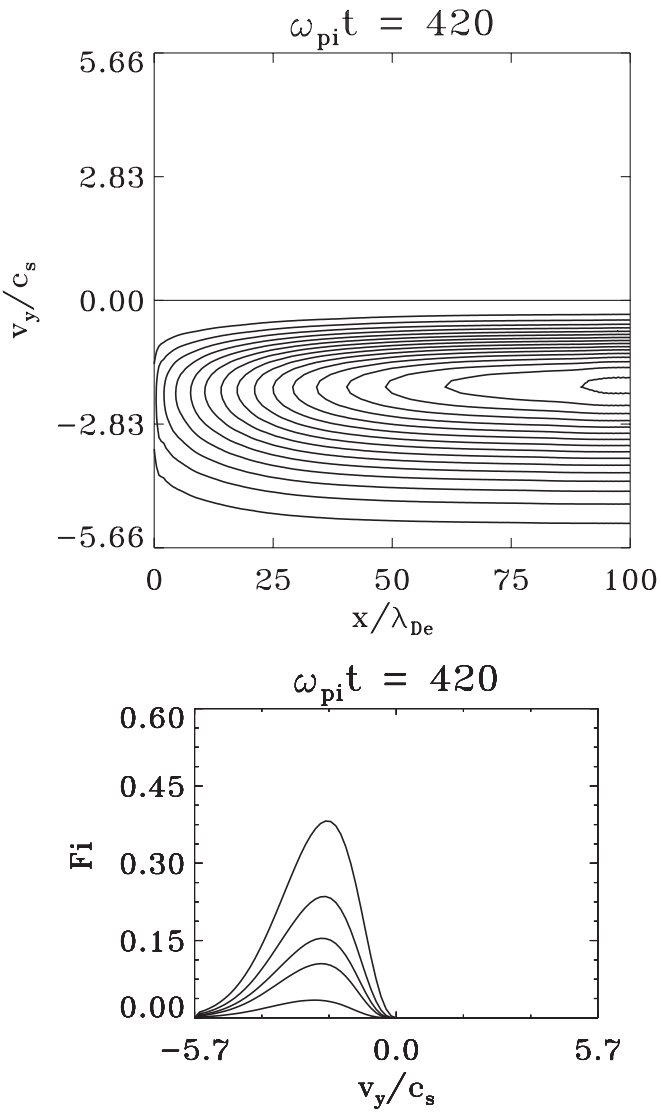

FIG. 13. Ion distribution functions $F_i(x,v_y)$ at $t=420$.

$$E_x|_{x=L} - E_x|_{x=0} = \int_0^L (n_i - n_e)dx = \sigma. \tag{10}$$

The system is initially neutral $n_i=n_e$. The boundary condition on E_x in Eq. (9) is used to solve for the potential at $x=0$ in Eq. (3). The resulting electric field at $x=L$, obtained from the solution of Eq. (3), is related to the electric field at $x=0$ and to the charge σ appearing in the system through Eq. (10). We verify that this equation is satisfied at every time step.

Equations (1)–(3) are solved using a method of fractional step, discussed, for instance, in Ref. 14. We run the code and let the initially neutral plasma evolve to a steady state. The motion of the ions is advanced with a time step of $\Delta t=0.04$, and the motion of the electrons is advanced with $\Delta t=0.005$ (ions are advanced by one time step for every eight time steps for the electrons). We use 200 grid points in space in a domain $L=100$ Debye lengths, and 80 grid points in each velocity space direction for the ions, with velocity extrema for the ions equal to ± 4 ion thermal velocities ($\pm 4\sqrt{T_i/T_e}$ the acoustic velocity c_s), and for the electrons, the velocity extrema vary between $+0.8\times 4$ electron thermal velocities and -1.2×4 electron thermal velocities (in order to center the grid in the region where the electron distribution is dominant) with 250 grid points in velocity space. For an arbitrary plasma profile, we have the following relations for the ion temperatures:

$$T_{ix,y,z}(x) = \frac{1}{n_i(x)} \int d\vec{v}(v_{x,y,z} - \langle v_{x,y,z}\rangle)^2 f_i(x,\vec{v}), \tag{11}$$

$$\langle v_{x,y,z}\rangle = \frac{1}{n_i(x)} \int d\vec{v} v_{x,y,z} f_i(x,\vec{v}). \tag{12}$$

III. RESULTS

The ratio of the ion gyroradius to the Debye length is given by

$$\frac{\rho_i}{\lambda_{\mathrm{De}}} = \sqrt{\frac{2T_i}{T_e}} \frac{1}{\omega_{ci}/\omega_{pi}}. \tag{13}$$

If we assume initially the ion distribution with $T_{ix}=T_{iz}=T_i$, then the factor $2T_i$ in the calculation of the gyroradius in Eq.

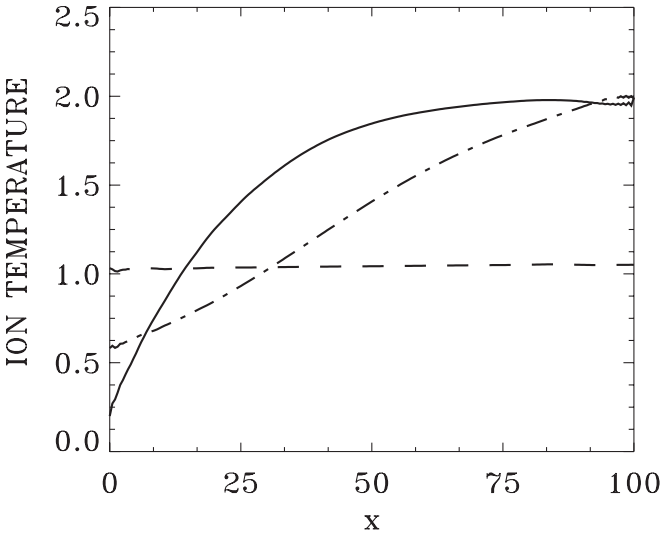

FIG. 14. $T_{ix}(x)$ (full curve), $T_{iy}(x)$ (dash curve), and $T_{iz}(x)$ (dash-dot curve) at $t=420$.

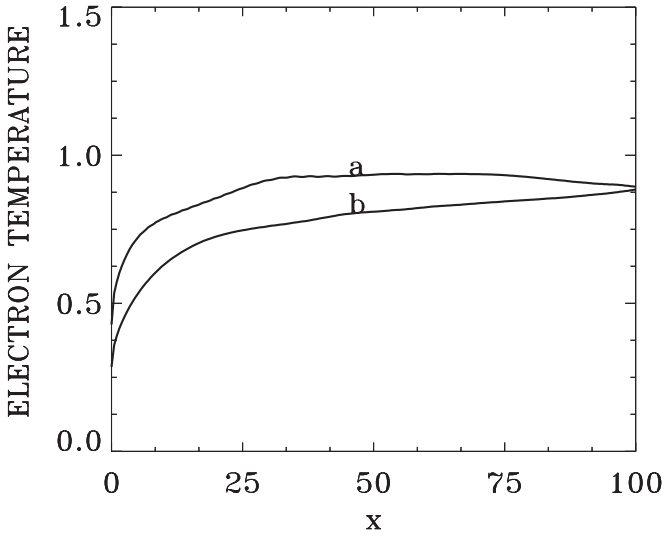

FIG. 15. Electron temperature $T_e(x)$ at (a) $t=370$ and (b) $t=420$.

(13) takes into account that the perpendicular temperature of the ions $\langle v_x^2\rangle+\langle v_z^2\rangle=2T_i/m_i$. The results we present are obtained for a small grazing angle of incidence of the magnetic field $\alpha=0.75°$. The total length L of the system is taken to be 100 Debye lengths. Three cases will be studied for the ratio of ρ_i/λ_{De}.

A. Case 1: $T_i/T_e=2$ and $\omega_{ci}/\omega_{pi}=0.1$

In this case, $\rho_i/\lambda_{De}=20$ and the length of the system is about 5 gyroradii (we recovered the same results by changing the length L to 150 Debye lengths and using 250 grid points in space). Preliminary results for this case were presented in Ref. 15. There exists a critical angle α_c where the transport of the ions perpendicular to the magnetic field is equal to the transport of the electrons parallel to the magnetic field (the x-components of the ion and electron velocities are equal to each other). Ions need half of a gyroperiod τ_i to travel twice the gyroradius ρ_i. In the time $\tau_i/2$, electrons will travel along the magnetic field a distance $\sqrt{T_e/m_e}\tau_i/2$. Hence, we have when we project in the x-direction

$$\tan\alpha_c=\frac{2\rho_i}{\sqrt{T_e/m_e}\tau_i/2}=\frac{2\sqrt{2T_i/m_i}\tau_i/(2\pi)}{\sqrt{T_e/m_e}\tau_i/2}=0.9\frac{\sqrt{T_im_e}}{\sqrt{T_em_i}}.$$

At this critical angle, the electrons moving along the magnetic field can still adjust to the gyration of the ions perpendicular to the magnetic field in their attempt to compensate for a charge separation. For the present set of parameters, there is a critical angle $\tan\alpha_c=0.9(T_im_e/T_em_i)^{1/2}=0.9/42.85$ or, equivalently, $\alpha_c=1.2°$. There are other effects such as gyrocooling, which reduces T_i and ρ_i in front of the wall, as discussed in Ref. 9, and polarization drift (toward the wall) from the accelerating electric field, which possibly do not exactly compensate so that the factor 0.9 might be approximate. In the present case, we have fixed $\alpha=0.75°$, therefore, $\alpha<\alpha_c$. Figure 1 shows the potential profile during a period of the evolution of the oscillation (at $t=350$, $t=375$, $t=400$, $t=425$, and $t=450$). The period of this oscillation for the present set of parameters is about 100, calculated from the numerical code. The electric field at the sheath entrance (the slope of the potential at $x=L$) oscillates between positive and negative values. We present in Fig. 2 the electric field profiles at $t=400$ and $t=450$. We present in Fig. 3 the electric field at the intermediate time $t=375$ (full curve), at a time where the slope of the potential at the sheath entrance is close to zero (see Fig. 1). The dotted curve in Fig. 3 plots the quantity $\nabla P_i/n_i$, where the pressure $P_i=0.5(n_iT_{ix}+n_iT_{iz})$. The dash-dot curve in Fig. 3 represents the Lorentz force in the x-direction for the ions, which in our units is written as $0.1\langle v_z\rangle/\cos\alpha$ (with $\omega_{ci}/\omega_{pi}=0.1$). The broken curve in Fig. 3 represents the combined force term $\nabla P_i/n_i+0.1\langle v_z\rangle/\cos\alpha$. The broken curve appears to follow the electric field curve, deviating only in front of the plate. (This deviation is due to the fact that n_i is small in front of the plate, so the division by n_i might cause some inaccuracy.) The results in Fig. 3 indicate that the observed oscillations take place around an equilibrium where the electric field bal-

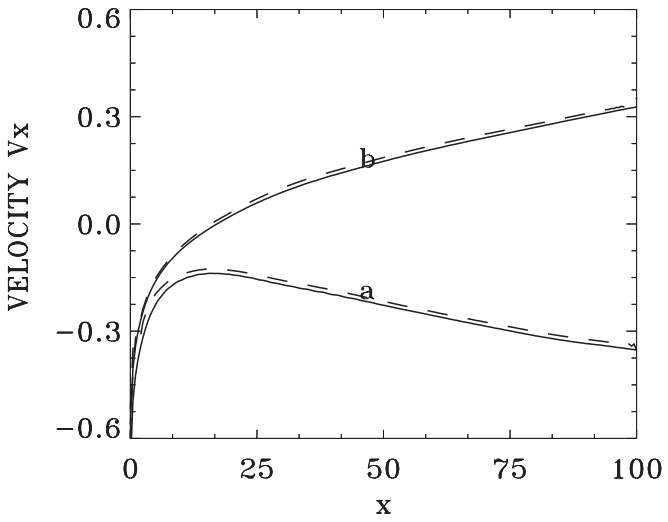

FIG. 16. Velocity $\langle v_x\rangle$ at (a) $t=370$ and (b) $t=420$ (ions full curves, electrons broken curves $\langle v_\parallel\rangle\sin\alpha$).

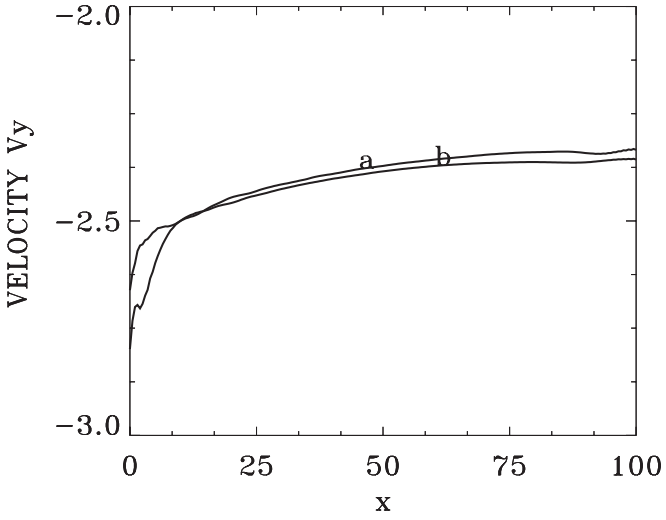

FIG. 17. Velocity $\langle v_y \rangle$ at (a) $t=370$ and (b) $t=420$.

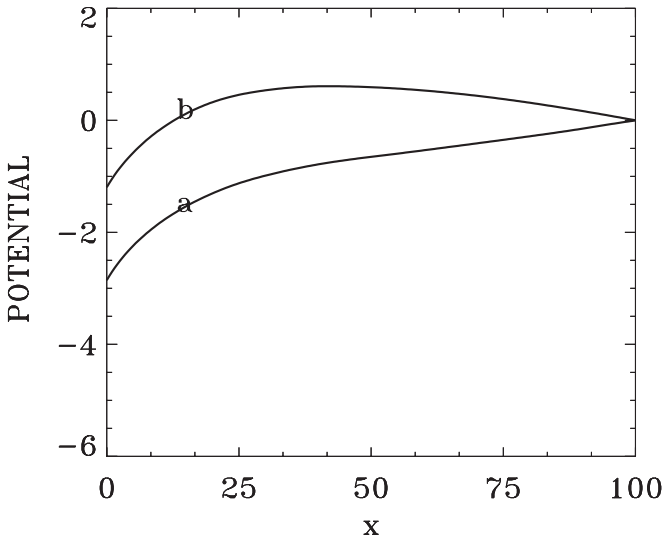

FIG. 19. Potential profile at (a) $t=290$ and (b) $t=340$.

ances the pressure force and the Lorentz force term. Figure 4 shows the density profiles (full curve electrons, broken curve ions) at $t=400$ and at $t=450$. The close agreement between the electron and ion density curves indicates that there is almost quasineutrality during this oscillation. The oscillation of the density curves reflects the fact that particles are allowed to move in and out at the right boundary of the domain during an oscillation period, maintaining quasineutrality during the oscillation and a total current of zero normal to the plate in the sheath domain. The currents normal to the plate are presented in Fig. 5 [full curve $J_{xe}=J_{e\|}\sin\alpha$ for the electrons, dotted curve J_{xi} for the ions, and the dash-dot curve for the difference $(J_{xi}-J_{e\|}\sin\alpha)$, which is essentially zero]. These curves are taken at $t=375$ and at $t=425$. The steady-state oscillation resulting from the ions motion and from the electrons running along the magnetic field takes place in such a way that the total current normal to the plate is zero from the sheath entrance at $x=L$ to the wall at $x=0$ and quasineutrality in the sheath is maintained (see Fig. 4). Since during steady-state oscillations the total current normal to the plate is zero, then Eq. (9) demands that $E_x|_{x=0}$ be constant at the wall, as observed in Fig. 2. On the other hand, we have $E_x|_{x=L}-E_x|_{x=0}=\sigma$ [see Eq. (10)]; therefore, the variation in the total charge σ in the sheath domain has to be followed by the same and equal variation in the electric field $E_x|_{x=L}$ at $x=L$. This is exactly what is observed in Fig. 2. Equation (10) is verified at every time step by the numerical code. Figure 6 represents the charge (n_i-n_e) at $t=400$ and $t=450$ (the two curves are close in the figure, but due to the large ratio of ρ_i/λ_{De}, a small variation in the charge separation translates into an effective large difference in the corresponding potential and electric field). There is a positive charge in front of the plate over a length of about 20 Debye lengths, i.e., over about 1 gyroradius. There is a tendency for the positive charge in front of the plate to decrease for small angles α and large ρ_i/λ_{De}, the electrons running along the magnetic field can reach closer to the wall, as discussed in Ref. 13. The energy fluxes $Q_i(x)$ and $Q_e(x)$ normal to the

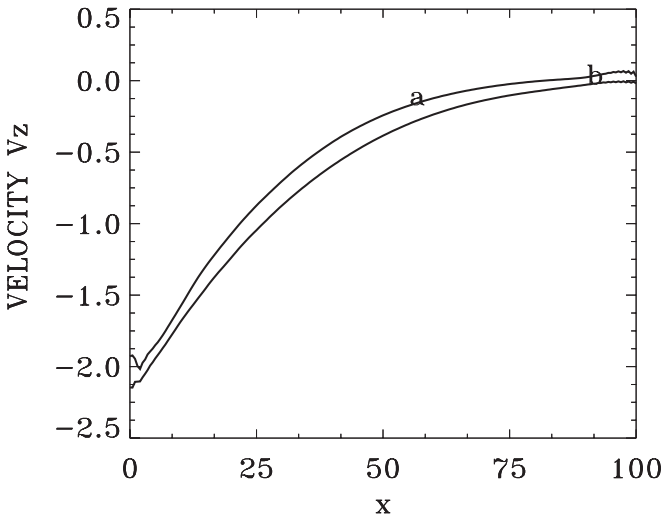

FIG. 18. Velocity $\langle v_y \rangle$ at (a) $t=370$ and (b) $t=420$.

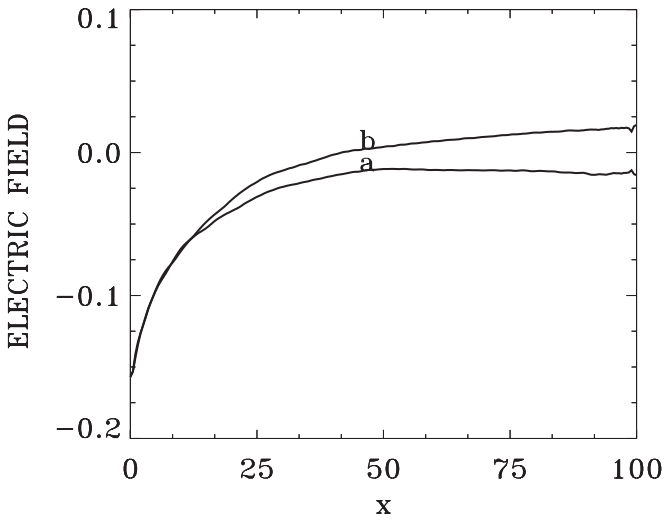

FIG. 20. Electric field at (a) $t=290$ and (b) $t=340$.

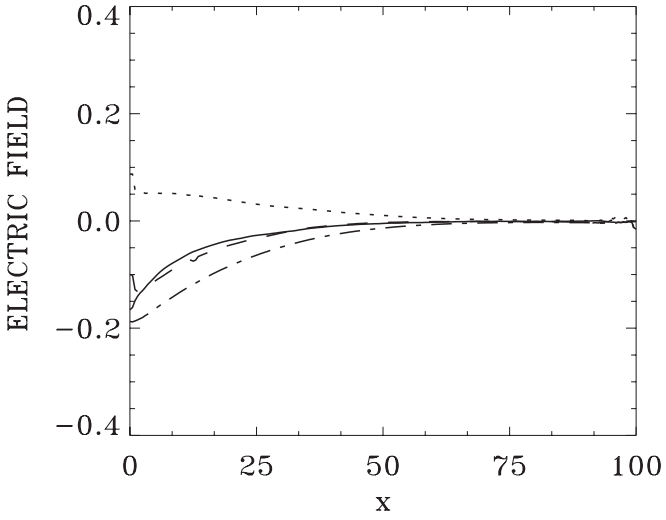

FIG. 21. Electric field at $t=315$ (full curve), $\nabla P_i/n_i$ (dotted curve), $0.1\langle v_z\rangle/\cos\alpha$ (dash-dot curve), and $\nabla P_i/n_i+0.1\langle v_z\rangle/\cos\alpha$ (dash curve).

wall for the ions and electrons are given in Fig. 7 and are defined by

$$Q_i(x) = \frac{1}{2}\int d\vec{v} v_x v^2 f_i(x,\vec{v}),$$

$$Q_e(x) = \frac{m_e}{m_i}\frac{1}{2}\sin\alpha\int dv_\parallel v_\parallel^3 f_e(x,v_\parallel) \tag{14}$$

(full curves for the electrons and broken curves for the ions at $t=375$ and $t=425$). Usually, at such a small grazing incidence of the magnetic field, the frozen electrons along the magnetic field will have tendency to prevent the transport of the ions across the magnetic field. However, we note during the oscillations of the ion energy flux (the broken curve in Fig. 7) that the ions maintain a contribution at the plate, reflecting the fact that a small population of ions are being scraped off in front of the wall. We can say that the oscillations act like a periodic pump for particles and energy, enforcing the necessary transport to the wall. A similar result was also reported in the experimental results presented in Ref. 16, which showed that the flux energy collected at the wall decreases with the angle of incidence of the magnetic field according to a sine law, goes through a minimum value at a critical angle of incidence, and below that critical angle of incidence, the flux energy collected at the wall was increasing again. However, the ratio of the ion gyroradius to the Debye length in the results reported in Ref. 16 was 200, so a comparison can be only qualitative. Figures 8 and 9 present the distribution function of the electrons for a half period interval at $t=370$ and $t=420$, showing the strong oscillation of the running electrons throughout the domain, especially at the sheath entrance at the right boundary and at the sheath wall at the left boundary in order to catch the ions

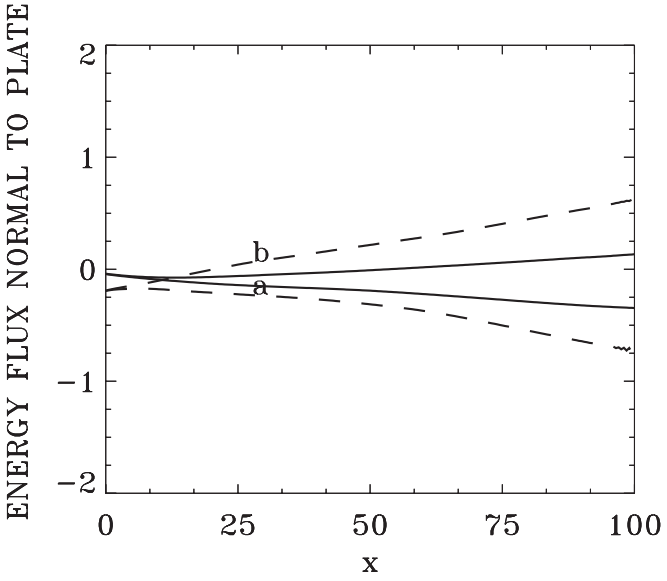

FIG. 23. Energy flux normal to the plate (Q_e full curves, Q_i dash curves) at (a) $t=375$ and (b) $t=425$.

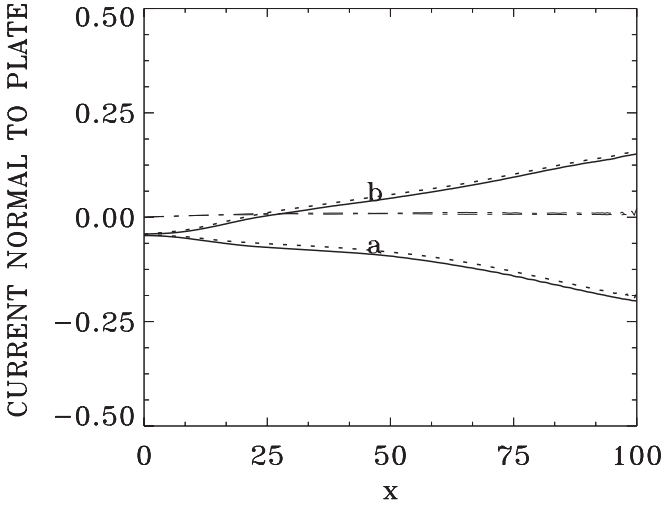

FIG. 22. Current normal to the plate (full curve electrons, dotted curve ions) at (a) $t=265$ and (b) $t=315$ (the dash-dot curve is the total current, essentially zero).

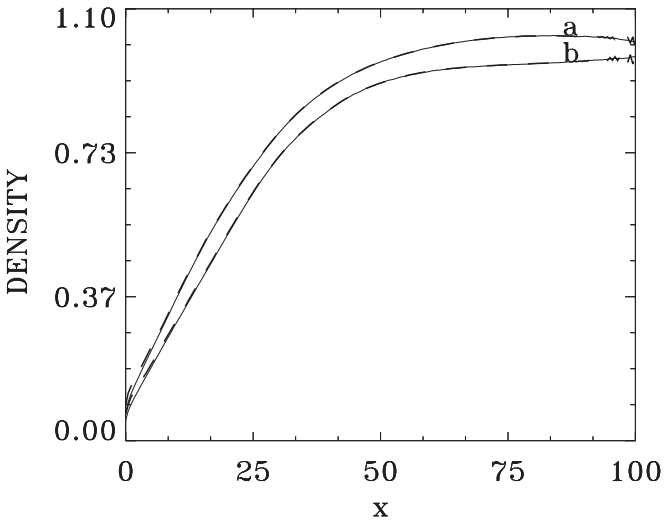

FIG. 24. Density profiles (full curve electrons, broken curve ions) at (a) $t=290$ and (b) $t=340$.

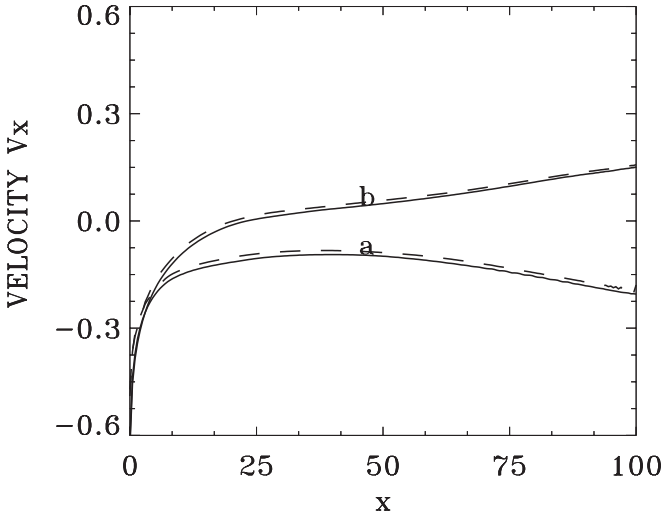

FIG. 25. Velocity $\langle v_x \rangle$ at (a) $t=265$ and (b) $t=315$ (ions full curves, electrons broken curves $\langle v_\parallel \rangle \sin \alpha$).

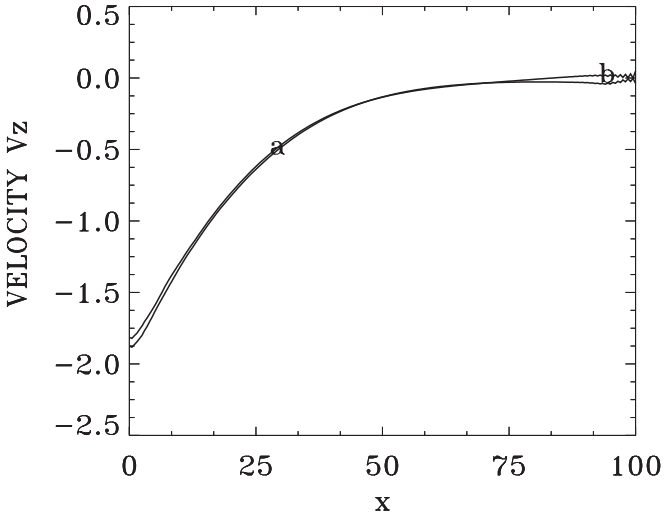

FIG. 27. Velocity $\langle v_z \rangle$ at (a) $t=265$ and (b) $t=315$.

and maintain quasineutrality and zero total current in the direction normal to the wall. Note also the marked and continuous deviations of the distribution functions from a symmetric Maxwellian (with a cutoff at the right edge), which can only be followed with the kinetic model for the electrons, showing that the adiabatic approximation is no longer applicable. The same oscillation is observed in the gyrating ion population in the x-direction in Figs. 10 and 11, where the 1D distribution function $F_i(x, v_x)$ is plotted

$$F_i(x, v_x) = \int dv_y dv_z f_i(x, \vec{v}). \tag{15}$$

The oscillating population of electrons and ions maintain quasineutrality and the equality of the ion and electron currents normal to the plate. Figures 12 and 13 represent $F_i(x, v_z)$ and $F_i(x, v_y)$ given by

$$F_i(x, v_{z,y}) = \int dv_x dv_{y,z} f_i(x, \vec{v}). \tag{16}$$

The distribution functions at the lower part of Figs. 8–13 are cuts obtained (from bottom to top) at $x=0$, $x=L/16$, $x=L/8$, $x=L/4$, and $x=L$ from the contour plots. When approaching the wall the width of the distribution function $F_i(x, v_z)$ in Fig. 12 shrinks (for the z-direction$\parallel \vec{E} \times \vec{B}$ drift). This gyrocooling effect described in Ref. 9 is due to the thermal energy gradually converted into kinetic energy of the wall-tangential drift motion. Note in Fig. 13 that the ions entering the sheath in the direction y (essentially parallel to the magnetic field since $\alpha=0.75°$) have a peak in the distribution function around the initial sound speed, $\sqrt{1+T_i/T_e}=1.732$ (see the bottom of Fig. 13). However, the distribution is not the initial Maxwellian distribution as in Eq. (4) (see again the bottom of Fig. 13, showing the distribution functions elongated in the negative direction). Figure 14 presents the ion temperature $T_{ix}(x)$ (full curve), $T_{iy}(x)$ (broken curve), and $T_{iz}(x)$ (dash-dot curve)

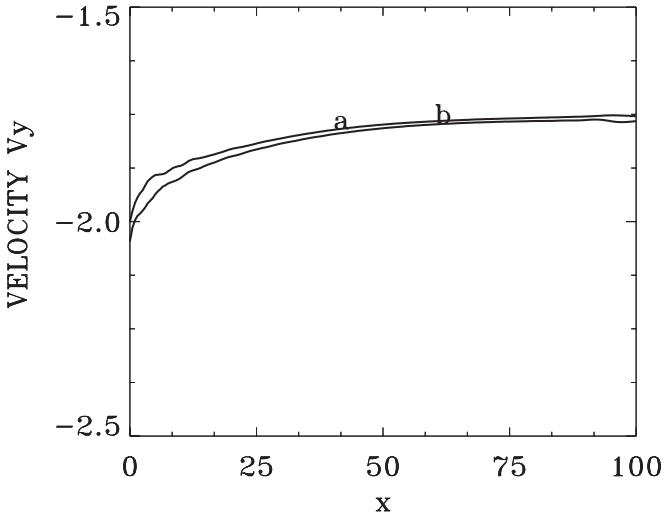

FIG. 26. Velocity $\langle v_y \rangle$ at (a) $t=265$ and (b) $t=315$.

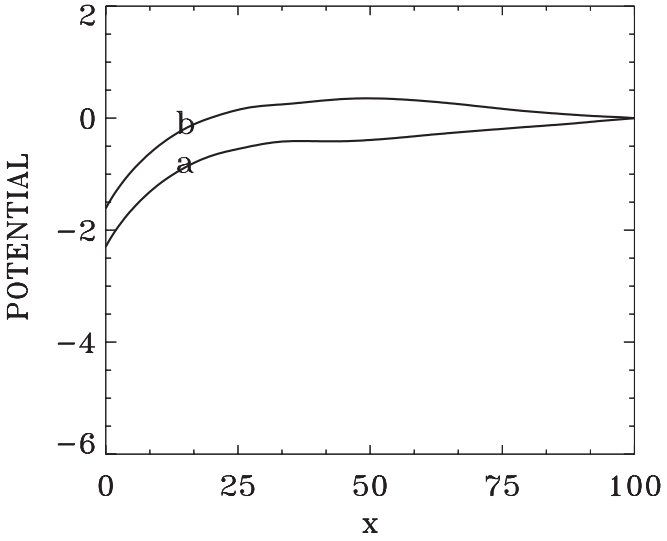

FIG. 28. Potential profile at (a) $t=212$ and (b) $t=214$.

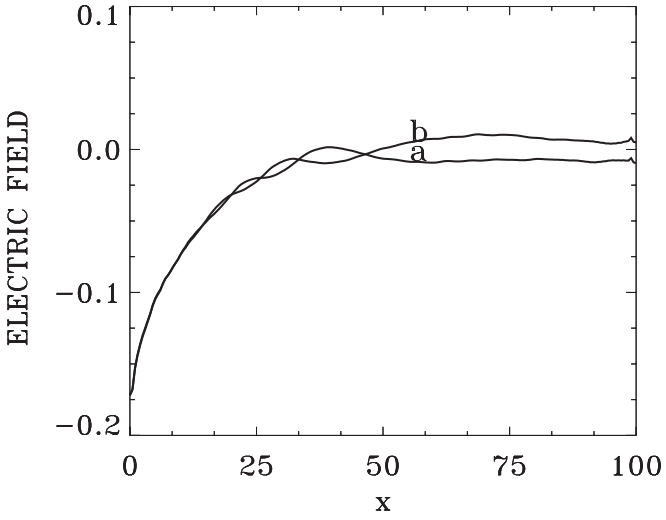

FIG. 29. Electric field at (a) $t=212$ and (b) $t=214$.

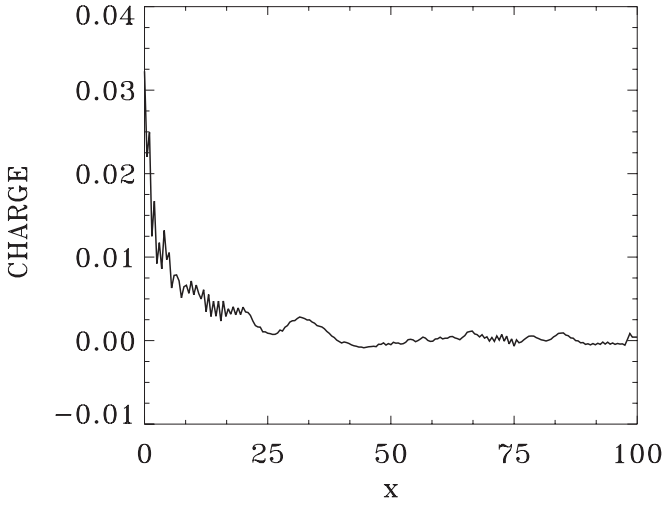

FIG. 31. Charge (n_i-n_e) at $t=213$.

[see Eq. (12)] at $t=420$. It is $T_{iz}(x)$ (dash-dot curve) which shows the most important variation during the oscillation. Note the cooling observed when approaching the wall for $T_{ix}(x)$ and $T_{iz}(x)$. Figure 15 presents the electron temperature $T_e(x)$ defined by

$$T_e(x) = \frac{1}{n_e(x)} \int dv_{\|}(v_{\|} - \langle v_{\|} \rangle)^2 f_e(x, v_{\|}) \tag{17}$$

(at $t=370$ and at $t=420$). It shows an oscillation that reflects the important oscillation of the electrons, and it also shows a cooling in front of the plate. Again, we see that an adiabatic approximation with a T_e constant in space and time is not possible.

Figures 16–18 present the ion velocities as calculated from Eq. (12). Also, we present in Fig. 16 the electron velocity in the x-direction $\langle v_{\|} \rangle \sin \alpha$ (broken curve), which, for the present small grazing angle of incidence, follow the variation in the ion velocity in the x-direction $\langle v_x \rangle$, thus maintaining quasineutrality and a zero total current normal to the plate in the x-direction during the steady-state oscillations. We note in Fig. 16, when we get close to the wall at $x=0$, that the oscillation of the ion velocity $\langle v_x \rangle$ normal to the wall tends to be replaced by a constant shape of the velocity $\langle v_x \rangle$ normal to the wall, as in a classical sheath. In Fig. 17 we see $\langle v_y \rangle$, which is essentially the velocity parallel to B since the angle α is very small, increasing slowly toward the wall. Although at the bottom curves in Fig. 13 the peak of the distribution functions $F_i(x, v_y)$ has the tendency to be located around the sound speed $\sqrt{1+T_i/T_e}=1.732$, the elongation of the distribution functions toward negative velocities in Fig. 13 results in a value of $\langle v_y \rangle$ at $x=L$ around 2.36 in Fig. 17. So the ions enter the sheath domain during the oscillation with an average velocity along the magnetic field at $x=L$, showing a very small oscillation around 2.36, which is not the sound velocity in this case. Finally, Fig. 18 shows the important increase in $\langle v_z \rangle$ parallel to the wall.

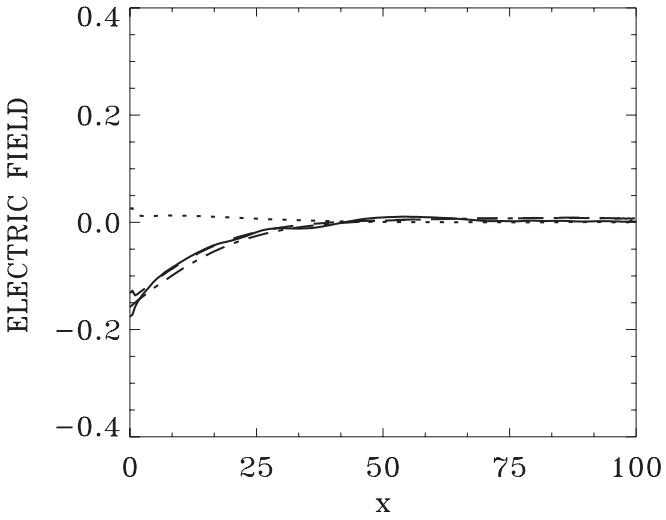

FIG. 30. Electric field at $t=213$ (full curve), $\nabla P_i/n_i$ (dotted curve), $0.1\langle v_z \rangle/\cos\alpha$ (dash-dot curve), and $\nabla P_i/n_i+0.1\langle v_z \rangle/\cos\alpha$ (dash curve).

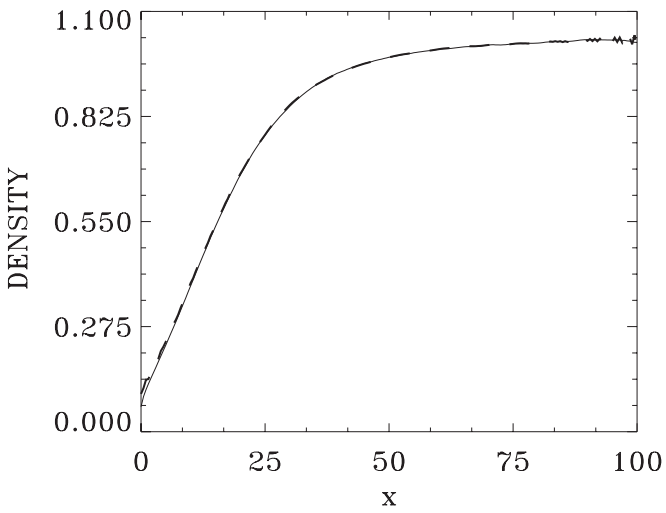

FIG. 32. Density profiles (full curve electrons, broken curve ions) at $t=213$.

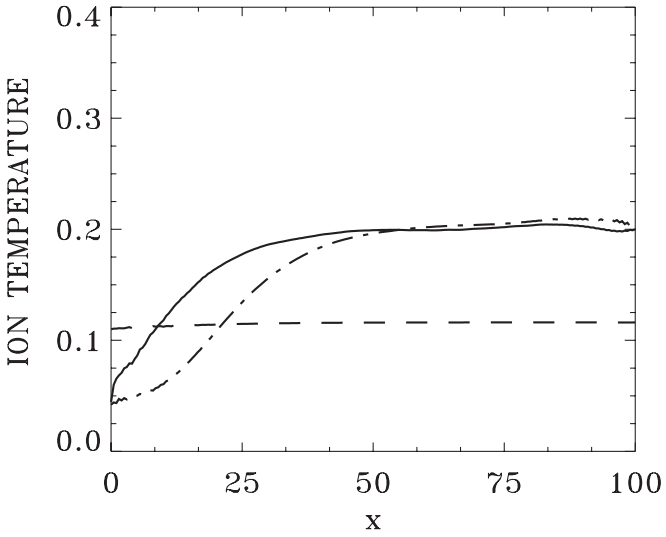

FIG. 33. $T_{ix}(x)$ (full curve), $T_{iy}(x)$ (dash curve), and $T_{iz}(x)$ (dash-dot curve) at $t=213$.

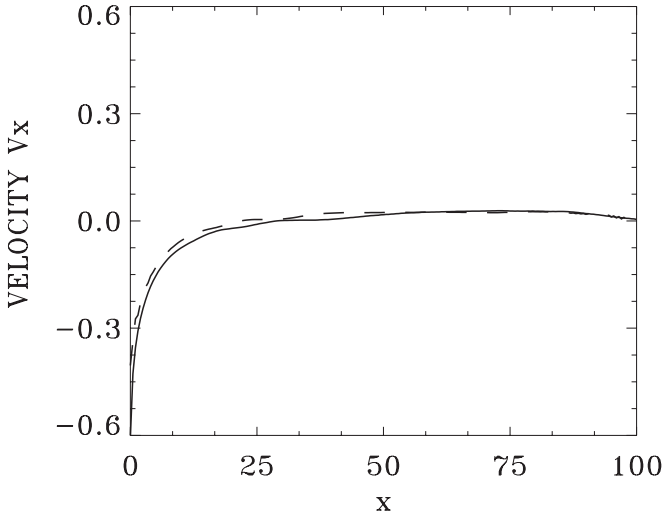

FIG. 35. Velocity $\langle v_x \rangle$ at $t=213$ (ions full curve, electrons broken curve $\langle v_{\|} \rangle \sin \alpha$).

B. Case 2: $T_i/T_e=1$ and $\omega_{ci}/\omega_{pi}=0.1$

In this case, $\rho_i/\lambda_{De}=14$ and the length of the system is about 7 gyroradii. We still keep $\alpha=0.75°$. The critical angle for the present set of parameters is $\alpha_c=0.85°$. The angle α is close to α_c, with $\alpha<\alpha_c$. Figures 19–27 summarize the results in this case. Oscillations are still present, but the amplitude of the oscillations has decreased (see Fig. 19 for the potential during a half period). The period of oscillation is still close to about 100. Note in Fig. 20 the electric field right next to the wall remaining essentially constant. However, the picture of a sheath with an electric field fading away as we move toward the right boundary is now modified by the appearance of small oscillations around the zero value of the electric field at the right boundary due to the kinetic treatment of the electrons, which are running to follow the ions, and maintaining zero total current in the direction normal to the wall and quasineutrality (see Figs. 22 and 24). We present in Fig. 21 the electric field at the intermediate time $t=315$ (full curve), at a time where the slope of the potential at the sheath entrance $x=L$ is close to zero (see Fig. 19). The dotted curve in Fig. 21 plots the quantity $\nabla P_i/n_i$, where the pressure $P_i=0.5(n_i T_{ix}+n_i T_{iz})$. The dash-dot curve in Fig. 21 represents the Lorentz force in the x-direction for the ions, which in our units is written as $0.1\langle v_z \rangle/\cos \alpha$. The broken curve in Fig. 21 represents the combined force term $\nabla P_i/n_i + 0.1\langle v_z \rangle/\cos \alpha$. The broken curve appears to follow the electric field curve. The results in Fig. 21 indicate that the observed oscillations take place around an equilibrium where the electric field balances the pressure force term and the Lorentz force term. In Fig. 22 electron and ion currents normal to the wall are equal so that the total current $(J_{xi}-J_{e\|} \sin \alpha)$ is zero. We note in Fig. 23 that the energy flux normal to the wall at the left boundary is slightly more negative with respect to Fig. 7. Note the density profiles in Fig. 24 being steeper close to the wall with respect to those presented in Fig. 4.

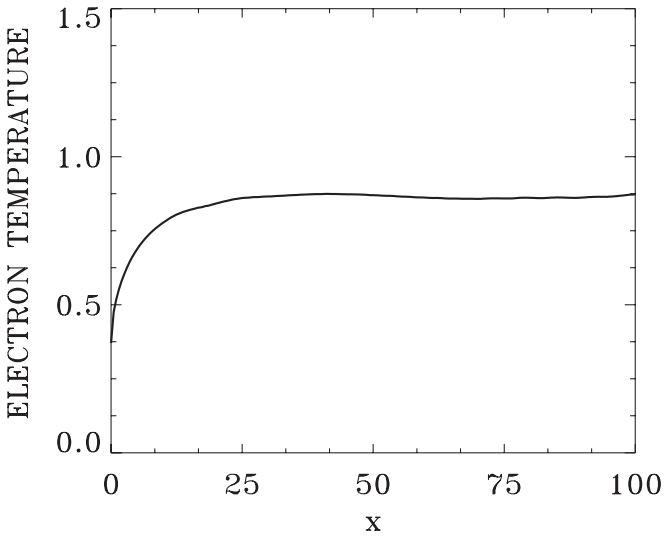

FIG. 34. Electron temperature $T_e(x)$ at $t=213$.

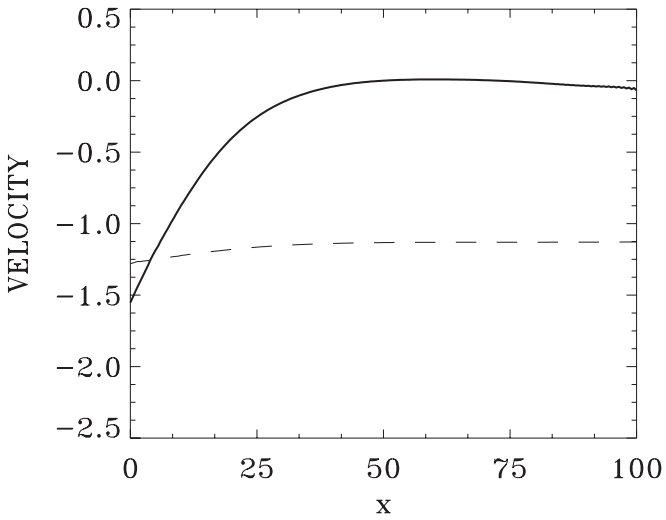

FIG. 36. Velocity at $t=213$ (dash curve $\langle v_y \rangle$, full curve $\langle v_z \rangle$).

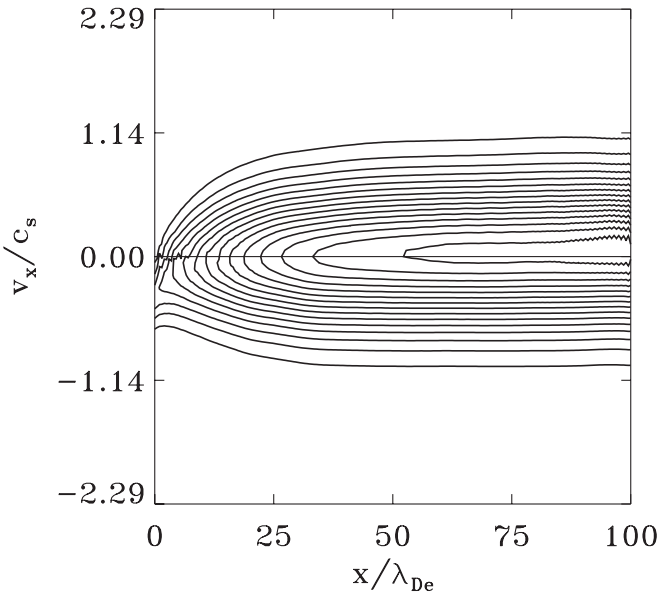

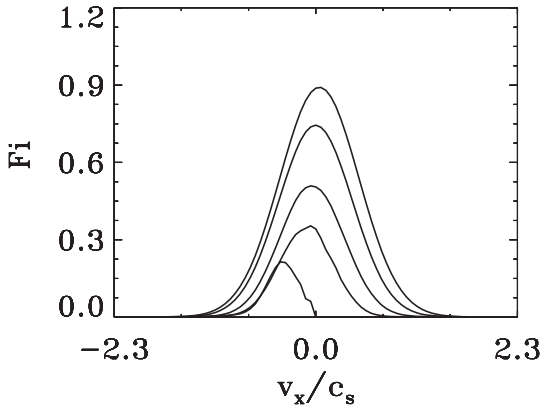

FIG. 37. Ion distribution functions $F_i(x, v_x)$ at $t=213$.

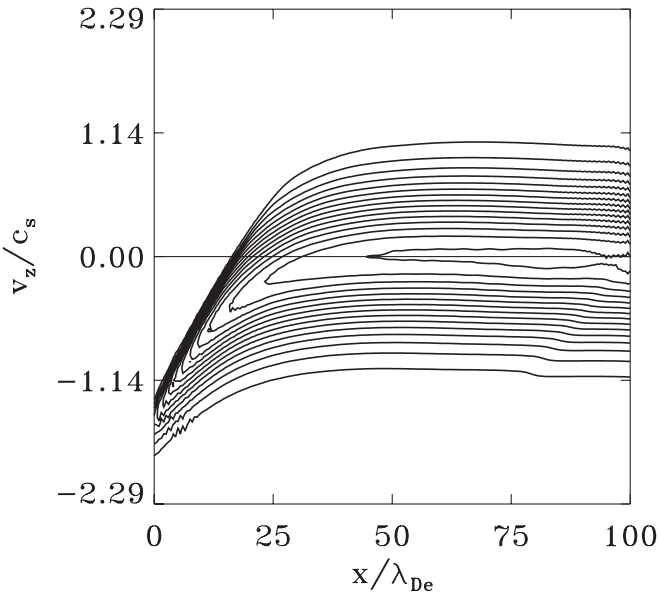

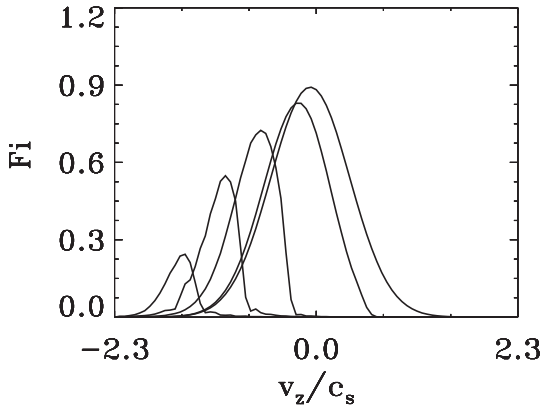

FIG. 38. Ion distribution functions $F_i(x, v_z)$ at $t=213$.

Figures 25–27 present the ion velocities as calculated from Eq. (12). We present also in Fig. 25 the electron velocity in the x-direction $\langle v_\parallel \rangle \sin\alpha$ (broken curve), which, for the present small grazing angle of incidence, follow the variation in the ion velocity in the x-direction $\langle v_x \rangle$, thus maintaining quasineutrality and a zero total current normal to the plate in the x-direction during the steady-state oscillations. In Fig. 25 the magnitude of the oscillation appears smaller than the equivalent one in Fig. 16. We note in Fig. 25, when we get close to the wall at $x=0$, that the oscillation of the ion velocity $\langle v_x \rangle$ normal to the wall tends to be replaced by a constant profile of the velocity $\langle v_x \rangle$ normal to the wall, as in a classical sheath. In Fig. 26 we see $\langle v_y \rangle$, which is essentially the velocity parallel to B since the angle α is very small, increasing slowly toward the wall. The velocity $\langle v_y \rangle$ at the entrance of the sheath at $x=L$ is essentially constant at -1.76, showing a negligible oscillation, while the sound speed in this case is $-\sqrt{1+T_i/T_e}=-1.414$. So the ions enter the sheath domain during the oscillation with an average velocity along the magnetic field at $x=L$ at -1.76, slightly lower than the sound velocity in the present case. Finally, Fig. 27 shows the important increase in $\langle v_z \rangle$ as ions accelerate toward the wall.

C. Case 3: $T_i/T_e=0.2$ and $\omega_{ci}/\omega_{pi}=0.1$

In this case, $\rho_i/\lambda_{De}=6.32$ and the length of the system is about 15 gyroradii. The critical angle in this case is $\alpha_c=0.38°$, below and not very close to the value $\alpha=0.75°$. In the present results, we are closer to a more familiar sheath behavior, as discussed, for instance, in Ref. 9. The results are presented in Figs. 28–40. Figure 28 shows the potential profiles and Fig. 29 shows the electric field at $t=212$ and $t=214$. A stable electric field profile appears in front of the wall, fades away as it penetrates the plasma region, and maintains a small oscillation around $x=L$. The period of the oscillation we see in this case is about 6 so at $t=214$ we have been through more than 30 periods of oscillation, yet the electric field profile in front of the wall is very stable. As in the previous cases, Eq. (10) is verified at every time step. For instance, in Fig. 30 the electric field at the sheath entrance $E_x|_{x=L}$ is close to zero at the intermediate time $t=213$. Then, from Eq. (10), we have $E_x|_{x=0} \approx -\sigma$, i.e., the charge collected on the wall is essentially equal and opposite to the charge appearing in the system. In Fig. 30 the electric field at the wall is -0.1730, and the integration over space of the charge in Fig. 31 (using a simple summation rule) is

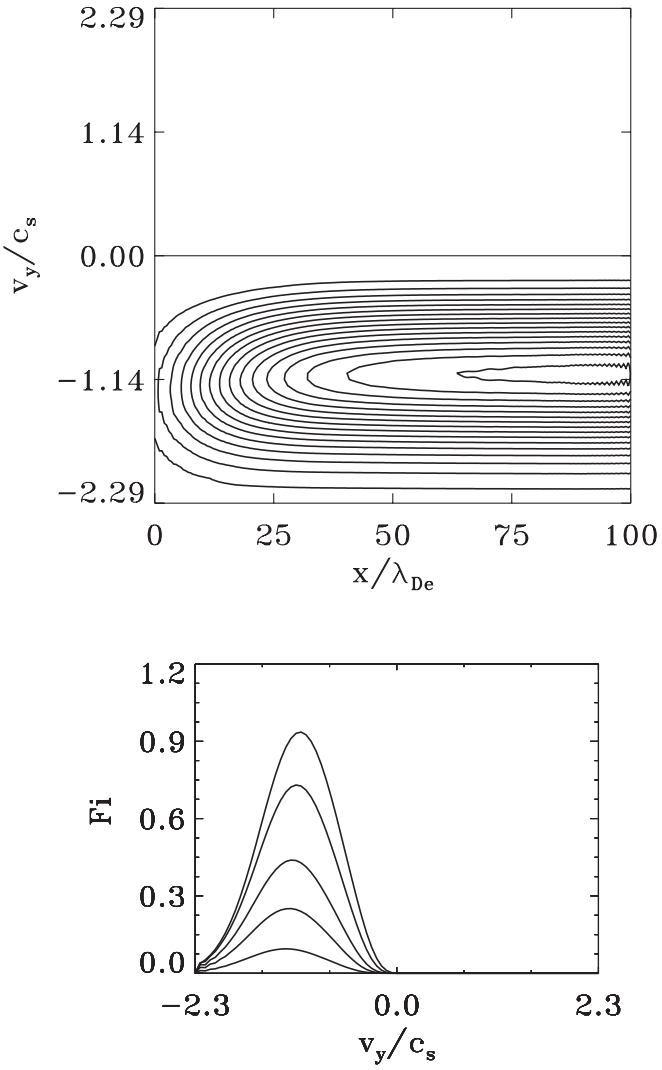

FIG. 39. Ion distribution functions $F_i(x,v_y)$ at $t=213$.

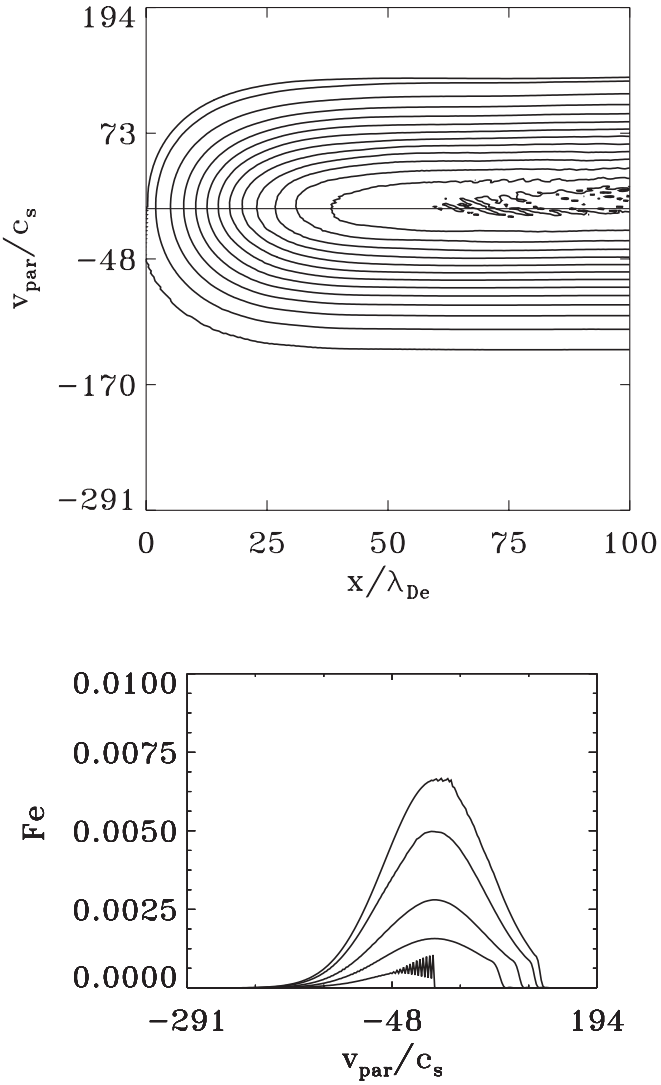

FIG. 40. Electron distribution functions $F_e(x,v_\parallel)$ at $t=213$.

0.171. The agreement is good. The electric field in Fig. 30 at the intermediate time $t=213$ [when the potential in Fig. 28 is in between curves (a) and (b)] follows nicely the broken curve $\nabla P_i/n_i+0.1\langle v_z\rangle/\cos\alpha$, especially in front of the wall where the profile of the electric field is constant. We note that the term $\nabla P_i/n_i$ (dotted curve) appears small in the present case so that the electric field essentially balances the Lorentz force term (the dash-dot curve). A small oscillation remains in the system, which is the result of the kinetic treatment of the electrons. The charge (n_i-n_e) is given in Fig. 31 and shows an accumulation of a positive charge in front of the wall more important than what was obtained in the first two cases and a deeper penetration of the charge separation in the plasma (in the first two cases the negative electrons can reach closer to the wall). The electron density (full curve) and ion density (broken curve) are given in Fig. 32.

The ion temperatures $T_{i,x,y,z}$, as defined in Eq. (9), are plotted in Fig. 33, and the electron temperature T_e is given in Fig. 34. Figures 35 and 36 show the ion velocities. In Fig. 35 the velocity $\langle v_x\rangle$ normal to the wall is negligibly small until close to the wall where $\langle v_x\rangle$ increases, directing the ions toward the wall as in a classical sheath. Also in Fig. 35 we see $\langle v_\parallel\rangle\sin\alpha$ for the electrons (dash curves). We see in Fig. 37 for the contour plot of $F_i(x,v_x)$ that the ions accelerate toward the wall in the x-direction. In Fig. 36 the $\langle v_y\rangle$ velocity (dash curve), essentially parallel to the magnetic field since α is very small, remains constant, and is equal to the initial sound speed $\sqrt{1+T_i/T_e}=1.095$, showing a very small increase closer to the plate. The distribution function $F_i(x,v_y)$ appears in Fig. 39 to remain close to its initial Maxwellian shape in the region toward the sheath entrance. In Fig. 36, $\langle v_z\rangle$ (full curve) shows an increase toward the plate, which is associated with a cooling in $F_i(x,v_z)$ toward the plate (see Fig. 38), which is termed gyrocooling in Ref. 9. Finally, Fig. 40 shows the electron distribution function $F_e(x,v_\parallel)$ at $t=213$. We note the accurate calculation of the distribution functions, especially close to the wall.

We have reached, with the present set of parameters, a solution where the ions penetrate along the magnetic field at the sound speed in what we can define as a magnetic presheath, maintain along the magnetic field a distribution very close to a Maxwellian distribution, and then are accelerated in front of the wall in the direction normal to the wall,

in what can be defined as the Debye sheath (see Fig. 35). These results are similar to what has been reported in Refs. 9, 11, and 17 using adiabatic electrons. In the present results, however, we are able to provide this solution at a high magnetic field and a small grazing angle of incidence using a kinetic equation for the electrons. Also the use of a kinetic equation for the electrons allows a small amplitude oscillation to persist, which is not present in the adiabatic electron approximation used in Refs. 9, 11, and 17.

IV. CONCLUSION

There is an abundant literature associated with plasma boundary and sheath problems where electrons are treated using an adiabatic law (see, for instance, Refs. 2, 9, and 11). In the results presented in Ref. 11 an accurate study was presented to distinguish between the collisional presheath, the magnetic presheath, and the Debye sheath in the plasma wall transition problem. It was found, however, that this distinction cannot be done in the case of a strong magnetic field, with $\rho_i/\lambda_{De} \gg 1$. In the present work, we have studied this problem using a kinetic description for the electrons, which are frozen along the magnetic field lines. We have presented a study of the physics associated with a collisionless plasma sheath, in the case of a strong magnetic field and with small grazing angles of incidence of the magnetic field, when the ions gyroradius is larger than the Debye length. In this case, the motion of the ions both along the magnetic field and normal to the wall is important. We have shown that below a critical angle of incidence α_c, the physics of the sheath differs from the classical sheath behavior obtained when the angle of incidence of the magnetic field α is greater than α_c. In the cases we have presented, the ratio of the ion gyroradius to the Debye length was varied from a relatively large value of 20, to 14, and to 6.32 at a constant angle of incidence of the magnetic field $\alpha=0.75°$. The electrons, frozen along the magnetic field lines, have to move rapidly along the magnetic field to try to catch the gyrating ions. This results in low frequency steady-state oscillations appearing in the system, an effect that is particularly important for the case when ρ_i/λ_{De} is large, as, for instance, the case $\rho_i/\lambda_{De}=20$ studied in Case 1, where large gyroradii ions can be scraped off by the wall. In these steady-state oscillations, the total current across the sheath remains zero. This undamped steady-state oscillations observed in the sheath with periods larger than the gyroperiod are due to the combined effect of the electrons running along the magnetic field lines and the ions gyrating across the magnetic field lines. These low frequency oscillations will have a tendency to be more complex in the presence of heavy impurity ions (which have larger gyroradii and larger gyroperiod) and are not related to edge turbulence. Note also the finite energy flux normal to the plate when $\alpha<\alpha_c$, as observed in Fig. 7. Usually the plasma particles are transported along the magnetic field lines. However, when the angle between the magnetic field and the wall is very small, the measurements of Langmuir probes in the boundary regions of fusion devices are enhanced with respect to what is predicted theoretically. The results in Ref. 16, done with $\rho_i/\lambda_{De}=200$, show that below a critical angle where the ion transport to the wall reaches a minimum, there is an increase in the ion transport to the wall. The present simulation results show how the physics of the sheath under the condition $\alpha<\alpha_c$ agrees, at least qualitatively, with these observations, and how it is difficult to distinguish in this case between sheath and presheath regions due to the strong oscillations in the sheath where we observe an important motion of the ions both along the magnetic field and normal to the plate.

The transition to the case with $\rho_i/\lambda_{De}=6.32$ and $\alpha>\alpha_c$ in Case 3 shows results closer to what one would expect in the case of a classical sheath: more important positive charge accumulating in front of the wall and the electric field reaching profiles that have stable negative peaks at the wall and fading away as we penetrate the plasma. The ions travel along the magnetic field at the sound speed in what can be defined as a presheath region, then their velocities are redirected toward the wall, and accelerated toward the wall under the effect of a constant electric field located in front of the wall, in what can be defined as a Debye sheath region.

In all the cases treated, the ions penetrate at $x=L$ with an average velocity along the magnetic field which has essentially a constant value, slightly larger (in absolute value) than the acoustic speed in the first two cases (see Figs. 17 and 26) and equal to the acoustic speed in the third case (see Fig. 36).

The low noise level of the Eulerian Vlasov code allows accurate calculation of the distribution functions and the associated charges and currents necessary to calculate the fields. We note the accurate calculations of the distribution functions, especially close to the wall. An accurate knowledge of the distribution functions at the wall is crucial to determine the effect of the ions on the material surface since sputtering and adsorption by the surface depend on the energy and angle of incidence of the ions impinging on it, as discussed, for instance, in Ref. 18.

With the use of a parallel-B kinetic equation for the electrons in the present work, rich physical processes in the sheath problem have been studied. It is beyond the scope of the present work to speculate about the importance of a second spatial dimension for this problem. The results presented in Ref. 19 with $\rho_i/\lambda_{De}=1$ point to the importance of the finite gyroradius effect in the plasma-wall transition problem. The results in Ref. 20 show the importance of the Kelvin–Helmholtz instabilities in the case of a two-dimensional plasma. The physics of the sheath problem in two spatial dimensions, with strong magnetic fields and grazing incidence (a problem of great importance in tokamak physics, for instance) is still to discover.

ACKNOWLEDGMENTS

M.S. is grateful to the IREQ computer center CASIR for computer time to do this work.

[1] F. Valsaque, G. Manfredi, J. P. Gunn, and E. Gauthier, Phys. Plasmas **9**, 1806 (2002).
[2] P. C. Stangeby, *Plasma Boundary of Magnetic Fusion Devices* (Institute of Physics, Bristol, 2000).
[3] D. Bohm, in *The Characteristics of Electrical Discharges in Magnetic Fields*, edited by A. Guthry and R. K. Wakerling (McGraw-Hill, New York, 1949), Chap. 3, p. 77.

[4]K.-U. Riemann, J. Phys. D **24**, 493 (1991).
[5]K.-S. Chung and I. H. Hutchinson, Phys. Rev. A **38**, 4721 (1988).
[6]D. Tskhakaya, B. Elliasson, P. K. Shukhla, and S. Kuhn, Phys. Plasmas **11**, 3945 (2004).
[7]M. Shoucri, Jpn. J. Appl. Phys., Part 1 **46**, 3045 (2007).
[8]R. Chodura, Phys. Fluids **25**, 1628 (1982).
[9]H. Gerhauser and H. A. Claassen, Contrib. Plasma Phys. **38**, 331 (1998).
[10]E. Ahedo, Phys. Plasmas **4**, 4419 (1997).
[11]S. Devaux and G. Manfredi, Phys. Plasmas **13**, 083504 (2006).
[12]D. Tskhakaya and S. Kuhn, Europhys. Conf. Abstr. **25A**, 1681 (2001); Plasma Phys. Controlled Fusion **47**, A327 (2005).
[13]M. Shoucri, H. Gerhauser, and K.-H. Finken, Phys. Scr. **75**, 712 (2007).
[14]M. Shoucri and R. Gagné, J. Comput. Phys. **27**, 315 (1978); M. Shoucri, *Numerical Solution of Hyperbolic Differential Equations* (Nova Science, New York, 2008).
[15]M. Shoucri, H. Gerhauser, and K.-H. Finken, Plasma Phys. Rep. **34**, 750 (2008).
[16]B. Koch, W. Bohmeyer, and G. Fussmann, J. Nucl. Mater. **337–339**, 211 (2005).
[17]D. Sharma, Phys. Plasmas **12**, 103506 (2005).
[18]R. J. Seeböck, Surf. Coat. Technol. **166–119**, 5643 (1999).
[19]G. Manfredi, M. Shoucri, I. Shkarofsky, P. Bertrand, A. Ghizzo, S. Krasheennikov, D. Sigmar, O. Batishchev, and A. Batishcheva, J. Nucl. Mater. **266–269**, 873 (1999).
[20]K. Teilhaber and C. K. Birdsall, Phys. Rev. Lett. **62**, 772 (1989); Phys. Fluids B **1**, 2244 (1989).